Supporting Information for "On the Kapitza Resistance Between Few-Layer Graphene and Water: Liquid Layering Effects"

Dmitry Alexeev,[1,*] Jie Chen,[1,2,3,*] Jens H. Walther,[1,4] Konstantinos P. Giapis,[5] Panagiotis Angelikopoulos,[1] and Petros Koumoutsakos[1,†]

[1] *Computational Science and Engineering Laboratory, Department of Mechanical and Process Engineering, ETH Zurich, CH-8092 Zurich, Switzerland*

[2] *Center for Phononics and Thermal Energy Science, School of Physics Science and Engineering, Tongji University, Shanghai 200092, China*

[3] *Institute for Advanced Study, Tongji University, Shanghai 200092, China*

[4] *Department of Mechanical Engineering, Technical University of Denmark, DK-2800 Kgs. Lyngby, Denmark*

[5] *Division of Chemistry and Chemical Engineering, California Institute of Technology, Pasadena, California 91125*

SIMULATION PROTOCOL

In this section we present the details on simulations we performed. Initially $N+2$ graphene layers of size $L \times L$ are placed along z axis with $d = 3.35$ Å spacing between each other. Followed is the water block of size $L \times L \times W$ and $N+2$ more graphene layers of the same size. The resulting system is mirrored with respect to a XY plane and shifted along Z such that distance d between graphene layers of the original system and its symmetric image is maintained. The schematic of the setup is shown in Fig. 1 of the *Main Text*.

Each simulation consists of three stages: equilibration to isothermal-isobaric (N, P, T) ensemble; applying temperature gradient at canonical ensemble (N, V, T); collecting the statistics at canonical ensemble while the temperature gradient is maintained. To achieve the temperature gradient, a high temperature Nosé-Hoover heat bath is applied to four central graphene layers and a low temperature Nosé-Hoover heat bath is applied to four outermost graphene layers (two leftmost and two rightmost). Periodic boundary conditions are applied in all directions. Equilibration always takes 400 ps. Applying temperature gradient takes from 1 ns to 3 ns depending on the number of used layers, and collecting the statistics takes from 2 ns to 3 ns.

Water was modeled with flexible simple point charge (SPC) model [1]. We also perform a simulation using rigid SPC water model [2]. The result are almost identical to the corresponding simulation with flexible water model: see Table S1.

Typical pressure evolution versus time is shown in the Fig. S3. High pressure oscillations are observed due to the high stiffness of both water and graphene. However, the average pressure remains constant.

DATA EXTRACTION

Kapitza resistance R_K was calculated as $R_K = \Delta T / J$, where ΔT is the temperature jump at the solid-liquid interface, and J is the heat flux through the interface. The heat flux is defined as the conducted energy from the high temperature heat bath to the low temperature heat sink per unit time across unit area. Due to the symmetry of our simulation setup (Fig. 1), the heat flux can be computed as half of the slope of the energy change with respective to time in the heat bath: $J = 0.5 \frac{d}{dt} \Delta E(t)$, where ΔE is induced energy in heat bath (Fig. S2). In our calculations, we average the local temperature in two symmetric copies. As shown in Fig. S1, ΔT is computed from the solid and liquid temperature at the interface. Solid temperature at the interface is determined by a linear fitting of the temperatures in different graphene layers. Water is divided into bins of 0.1 Å in thickness along z, thus liquid temperature at the interface is determined by fitting the temperatures of water in different bins on a straight line. The error in Kapitza resistance is given by errors of two linear fits.

Important to note that with the described procedure, we calculate two Kapitza resistances – one at a high temperature interface, and the other at a low temperature interface (Fig. S1). In all our simulation, the low temperature Kapitza resistance is consistently about 10% larger than high temperature one. We always report the average over these two and the full set of data is available in Table S1.

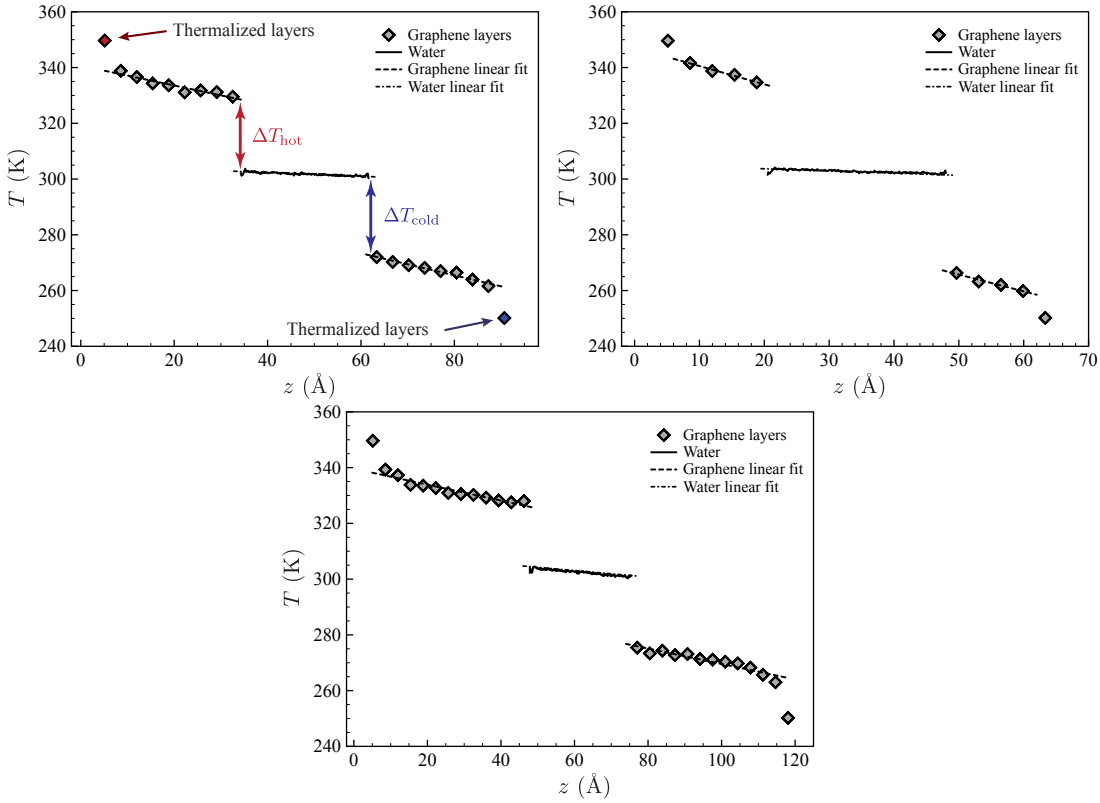

Figure S1. Temperature profiles of the systems with $N = 8$, $N = 4$, $N = 12$. Two temperature jumps: $\Delta T_{\rm hot}$ and $\Delta T_{\rm cold}$ correspond to two interfaces between water and graphene. Linear fitting is used to suppress thermal oscillations and to extrapolate water temperature up to the first graphene sheet. Simulation parameters are as follows: $L = 60$ Å, $W = 30$ Å, $T = 300$ K, $\delta = 100$ K, $P = 1$ bar, $\phi = 95^\circ$.

TEMPERATURE DEPENDENCE

The applied temperature difference δ has a minor effect on the averaged calculation results of the Kapitza resistance R_K, but affects significantly the accuracy of the results (Fig. S5(a)). To suppress the standard deviation of the predications, we use $\delta = 100$ K in our production runs. We also find that R_K is independent of the cross section size when $L > 4$ nm (Fig. S5(b)). Moreover, we observe that the R_K decreases with temperature T (Fig. S5(c)), which is consistent with previous experimental and theoretical studies [3, 4].

WATER STRUCTURE IN THE DENSITY PEAK

Fig. S4 shows the 2D Radial Distribution Function (RDF) of oxygen atoms located at the water density peak. Negligible change in RDF was observed for different contact angles.

---

* These authors contributed equally to this work.
† Electronic address: petros@ethz.ch

[1] Wu, Y.; Tepper, H. L.; Voth, G. A. *J. Chem. Phys.* **2006**, *124*, 024503.
[2] Berendsen, H. J. C.; Grigera, J. R.; Straatsma, T. P. *J. Phys. Chem.* **1987**, *91*, 6269-6271.
[3] Pollack, G. L. *Rev. Mod. Phys.* **1969**, *41*, 48-81.
[4] Stoner, R. J.; Maris, H. J. *Phys. Rev. B* **1993**, *48*, 16373-16387.

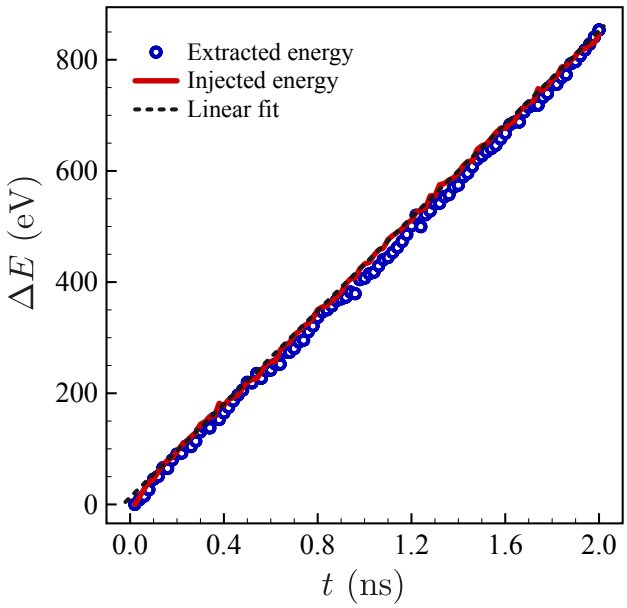

Figure S2. Additional energy ΔE introduced by Nosé-Hoover heat baths during the third stage of simulation.

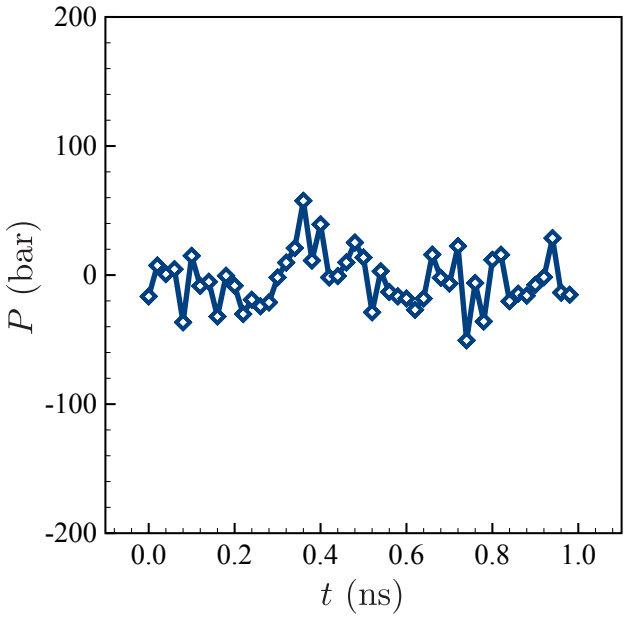

Figure S3. Pressure P evolution over the course of the run. Simulation parameters are as follows: $N = 8$, $L = 60$ Å, $W = 30$ Å, $T = 300$ K, $\delta = 100$ K, $P = 1$ bar, $\phi = 95°$.

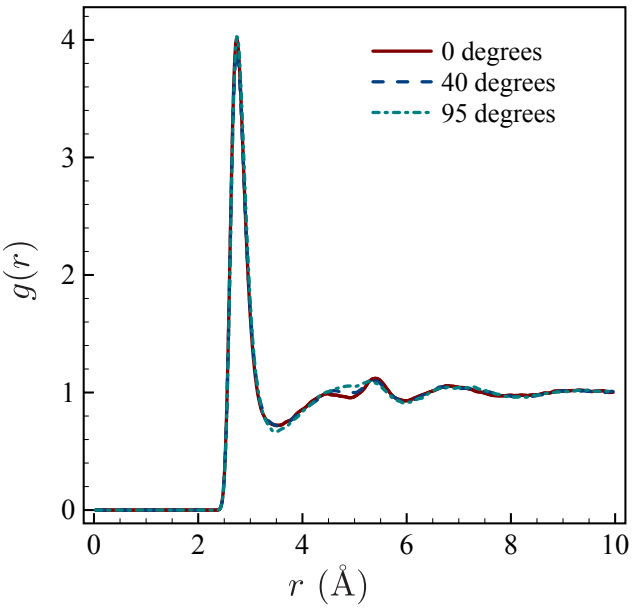

Figure S4. 2D radial distribution function $g(r)$ of oxygen atoms in the water peak. We observe negligible difference with respect to wetting properties of the interface. Simulation parameters are as follows: $N = 8$, $L = 60$ Å, $W = 30$ Å, $T = 300$ K, $\delta = 100$ K, $P = 1$ bar.

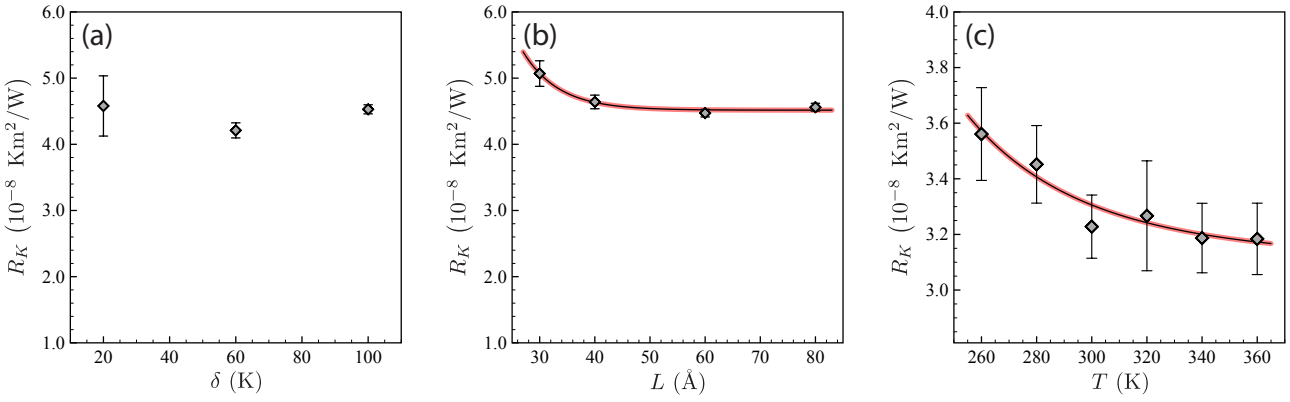

Figure S5. Dependance of the Kapitza resistance R_K on: (a) applied temperature difference δ ($N = 4$ here) (b) system cross-section size L ($N = 4$ here) and (c) average system temperature T ($N = 8$ here).

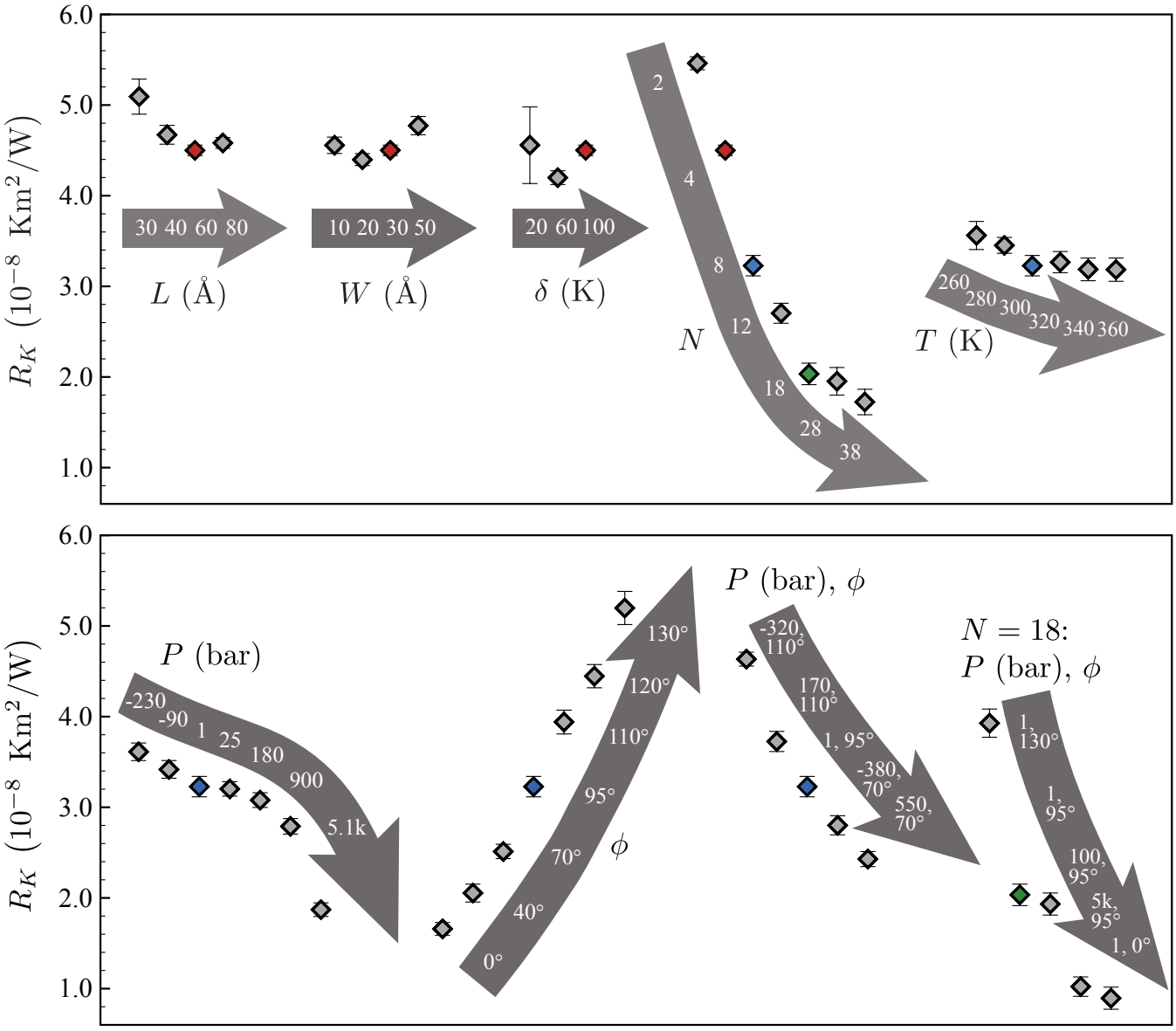

Figure S6. Overlook of all the simulations performed. Numbers on the arrows correspond to change in values, mentioned at the corresponding arrow. Three reference ambient simulations are represented by colored diamonds:
red: $N = 4$, $W = 3$ nm, $L = 6$ nm, $T = 300K$, $\delta = 100$ K, $P = 1$ bar, $\phi = 95°$;
blue: $N = 8$, $W = 3$ nm, $L = 6$ nm, $T = 300K$, $\delta = 100$ K, $P = 1$ bar, $\phi = 95°$;
green: $N = 18$, $W = 3$ nm, $L = 6$ nm, $T = 300K$, $\delta = 100$ K, $P = 1$ bar, $\phi = 95°$.

TABLE S1. Data for all performed simulations.

Run	Water model	N	W (Å)	L (Å)	T (K)	δ (K)	P (bar)	ϕ (deg)	R_K (Km^2/W)	Std. (Km^2/W)
1	Flexible	4	30	30	300	100	1	95	5.093×10^{-8}	1.936×10^{-9}
2	Flexible	4	30	40	300	100	1	95	4.672×10^{-8}	1.040×10^{-9}
3	Flexible	4	30	40	300	20	1	95	5.124×10^{-8}	5.000×10^{-9}
4	Flexible	4	10	60	300	100	1	95	4.556×10^{-8}	9.003×10^{-10}
5	Flexible	4	20	60	300	100	1	95	4.398×10^{-8}	6.628×10^{-10}
6	Flexible	8	30	60	260	100	1	95	3.561×10^{-8}	1.550×10^{-9}
7	Flexible	8	30	60	280	100	1	95	3.452×10^{-8}	8.732×10^{-10}
8	Flexible	8	30	60	300	100	10	95	3.203×10^{-8}	7.967×10^{-10}
9	Flexible	8	30	60	300	100	1	110	3.940×10^{-8}	1.313×10^{-9}
10	Flexible	8	30	60	300	100	1	120	4.446×10^{-8}	1.281×10^{-9}
11	Flexible	8	30	60	300	100	1	95	3.228×10^{-8}	1.125×10^{-9}
12	Flexible	12	30	60	300	100	1	95	2.703×10^{-8}	1.100×10^{-9}
13	Flexible	18	30	60	300	100	1	95	2.034×10^{-8}	1.185×10^{-9}
14	Flexible	2	30	60	300	100	1	95	5.461×10^{-8}	7.121×10^{-10}
15	Flexible	4	30	60	300	100	1	95	4.500×10^{-8}	5.788×10^{-10}
16	Flexible	8	30	60	300	100	1	0	1.659×10^{-8}	7.037×10^{-10}
17	Flexible	8	30	60	300	100	1	130	5.198×10^{-8}	1.827×10^{-9}
18	Flexible	8	30	60	300	100	1	160	1.872×10^{-7}	4.861×10^{-9}
19	Flexible	8	30	60	300	100	1	40	2.054×10^{-8}	9.851×10^{-10}
20	Flexible	8	30	60	300	100	1	70	2.513×10^{-8}	7.880×10^{-10}
21	Flexible	28	30	60	300	100	1	95	1.952×10^{-8}	1.524×10^{-9}
22	Flexible	38	30	60	300	100	1	95	1.724×10^{-8}	1.405×10^{-9}
23	Flexible	18	30	60	300	100	1	0	8.946×10^{-9}	1.219×10^{-9}
24	Flexible	18	30	60	300	100	1	130	3.928×10^{-8}	1.555×10^{-9}
25	Flexible	8	30	60	300	100	170	110	3.726×10^{-8}	1.110×10^{-9}
26	Flexible	8	30	60	300	100	180	95	3.079×10^{-8}	8.091×10^{-10}
27	Flexible	8	30	60	300	100	-230	95	3.612×10^{-8}	9.688×10^{-10}
28	Flexible	8	30	60	300	100	-320	110	4.634×10^{-8}	7.685×10^{-10}
29	Flexible	8	30	60	300	100	-380	70	2.801×10^{-8}	1.051×10^{-9}
30	Flexible	18	30	60	300	100	5000	95	1.022×10^{-8}	1.072×10^{-9}
31	Flexible	8	30	60	300	100	5100	95	1.871×10^{-8}	7.508×10^{-10}
32	Flexible	8	30	60	300	100	550	70	2.429×10^{-8}	8.279×10^{-10}
33	Flexible	8	30	60	300	100	900	95	2.790×10^{-8}	8.611×10^{-10}
34	Flexible	8	30	60	300	100	-90	95	3.418×10^{-8}	9.756×10^{-10}
35	Flexible	4	30	60	300	20	1	95	4.557×10^{-8}	4.230×10^{-9}
36	Flexible	4	30	60	300	60	1	95	4.199×10^{-8}	7.577×10^{-10}
37	Flexible	8	30	60	320	100	1	95	3.267×10^{-8}	1.169×10^{-9}
38	Flexible	4	50	60	300	100	1	95	4.773×10^{-8}	1.005×10^{-9}
39	Flexible	4	30	80	300	100	1	95	4.582×10^{-8}	5.917×10^{-10}
40	Flexible	4	30	80	300	20	1	95	3.326×10^{-8}	5.081×10^{-9}
41	Flexible	18	30	60	300	100	100	95	1.933×10^{-8}	1.216×10^{-9}
42	Flexible	8	30	60	340	100	1	95	3.187×10^{-8}	1.253×10^{-9}
43	Flexible	8	30	60	360	100	1	95	3.184×10^{-8}	1.284×10^{-9}
44	Rigid	8	30	60	300	100	1	95	3.297×10^{-8}	1.125×10^{-9}